

Article

## The Superiority of Tsallis Entropy over Traditional Cost Functions for Brain MRI and SPECT Registration

Henrique Amaral-Silva <sup>1,\*</sup>, Lauro Wichert-Ana <sup>1,2,3,5</sup>, Luiz Otavio Murta <sup>4</sup>,  
Larissa Romualdo-Suzuki <sup>6</sup>, Emerson Itikawa <sup>2,3</sup>, Geraldo Filho Bussato <sup>5</sup>  
and Paulo Azevedo-Marques <sup>1,3</sup>

<sup>1</sup> Center of Imaging Sciences and Medical Physics, Internal Medicine Department and Graduate Program, Ribeirão Preto Medical School, University of São Paulo, Ribeirão Preto 14049-900, Brazil; E-Mails: lwichert@fmrp.usp.br (L.W.-A.); pmarques@fmrp.usp.br (P.A.-M.)

<sup>2</sup> Nuclear Medicine Section, Ribeirão Preto Medical School, University of São Paulo, Ribeirão Preto 14049-900, Brazil; E-Mail: emerson.fm.usp@gmail.com

<sup>3</sup> Bioengineering Interunits Graduate Program, São Carlos School of Engineering, University of São Paulo, São Carlos 13566-590, Brazil

<sup>4</sup> Department of Computing and Mathematics, University of São Paulo, Ribeirão Preto 14040-901, Brazil; E-Mail: murta@usp.br

<sup>5</sup> The Center Interdisciplinary Research on Applied Neurosciences (NAPNA), University of São Paulo, São Paulo 05403-010, Brazil; E-Mail: geraldo.busatto@hc.fm.usp.br

<sup>6</sup> Department of Computer Science, University College London, London WC1E 6BT, UK; E-Mail: larissa.romualdo.11@ucl.ac.uk

\* Author to whom correspondence should be addressed; E-Mail: henrique.t.doamaralsilva@ieee.org; Tel.: +55-016-3602-2647; Fax: +55-016-3602-2648.

Received: 31 January 2014; in revised form: 25 February 2014 / Accepted: 12 March 2014 /

Published: 21 March 2014

---

**Abstract:** Neuroimage registration has an important role in clinical (for both diagnostic and therapeutic purposes) and research applications. In this article we describe the applicability of Tsallis Entropy as a new cost function for neuroimage registration through a comparative analysis based on the performance of the traditional approaches (correlation based: Entropy Correlation Coefficient (ECC) and Normalized Cross Correlation (NCC); and Mutual Information (MI) based: Mutual Information using Shannon Entropy (MIS) and Normalized Mutual Information (NMI)) and the proposed one based on MI using Tsallis entropy (MIT). We created phantoms with known geometric transformations using Single Photon Emission Computed Tomography (SPECT) and Magnetic Resonance

Imaging from 3 morphologically normal subjects. The simulated volumes were registered to the original ones using both the proposed and traditional approaches. The comparative analysis of the Relative Error (RE) showed that MIT was more accurate in the intra-modality registration, whereas for inter-modality registration, MIT presented the lowest RE for rotational transformations, and the ECC the lowest RE for translational transformations. In conclusion, we have shown that, with certain limitations, Tsallis Entropy has application as a better cost function for reliable neuroimage registration.

**Keywords:** neuroimaging; registration; SPECT; MRI; mutual information; Tsallis entropy

---

## 1. Introduction

Systems for Computer Aided Diagnosis (CAD) have received significant attention as an auxiliary tool in medical diagnosis. In particular, CAD may contribute to the qualitative and quantitative analysis of medical images. For this, several image processing techniques must be applied for the realignment, registration, segmentation, normalization and smoothing of 2-D images and 3-D volumes [1,2]. The registration comprises the overlaying of two or more images using the coordinate system of one of them to establish correspondence to the coordinate system in the other one. This process can be performed in three ways: (a) manually, guided by a physician or a specialist who needs to drive the reference volume to the target one; (b) semi-automated registration, based on markers defined in the image content; and (c) automated registration, using algorithms that can be based on fiducial marks, surface matching, and similarity measures [3,4]. Rigid body registration is widely used for intra-subject neuroimage registration and it consists of searching rotations and translations to match images with the same anatomy; for instance, a 3D-to-3D rigid body registration is defined by three translations and three rotations, *i.e.*, six transformation parameters [5].

Based on clinical grounds, the findings obtained by different imaging techniques can be used in a complementary manner by physicians. The combination of morphologic images (X-ray, Ultrasound (US), Computed Tomography (CT) and Magnetic Resonance Imaging (MRI)) and the functional ones (Positron Emission Tomography (PET), Single Photon Emission Computed Tomography (SPECT) and functional Magnetic Resonance Imaging (fMRI)) can improve the image interpretation [6]. This procedure, known as multimodal or intermodal medical image registration, is a relevant tool for the surgical planning. In neurosurgery, for example, multimodal or intermodal image registrations are useful to identify lesions or to localize dysfunctional areas to be resected. For epilepsy, the multimodal registration of MRI and SPECT can provide important information for the localization of the epileptogenic zone that must be surgically removed for patients to be seizure-free [7]. Monomodal or intramodal registration are useful in the pre and post-condition image analysis, e.g., comparative inspection of the ictal and interictal SPECT images, subtraction of ictal and interictal SPECT co-registered to MRI (SISCOM), and for the study of ongoing or stepwise brain changes in the course of a disease [8]. Another interesting application of SPECT registration can be found on Oliveira *et al.* [9] in which is proposed a computational solution to quantify a specific to a non-specific uptake ratio in

[<sup>123</sup>I]FP-CIT SPECT images and simultaneously measure the spatial dimensions of the basal ganglia.

Currently many software solutions and methods are available for different registration applications. A very recent review about registration methods can be found in Oliveira *et al.* [10]. The well-known Statistical Parametric Mapping (SPM) adopts similarity measures for neuroimage registration, and gives four cost function options: Entropy Correlation Coefficient (ECC), Normalized Cross Correlation (NCC), standard Mutual Information using Shannon Entropy (MIS) and Normalized Mutual Information (NMI). Mutual Information (MI) is a measurement originated from Information Theory [11], and was first proposed for medical image registration in [12,13]. Thenceforward, many studies have found satisfactory results for registration based on Information Theory. Recently, a comparative study of 16 registration methods evaluated the multimodal rigid body registration of neuroimages. The results have shown that two methods based on MI were superior to the alternatives and obtained similar accuracy to that of the gold standard [14]. The most important contribution of MI is the use of entropy as a quantification of information.

The entropy of an image is understood as a measure of diffusion of a gray level distribution. A homogeneous image have low entropy value since its histogram has just one peak; in the other hand, a heterogeneous image, with many peaks in its histogram, result in a high entropy value [15]. In this setting, given two images A and B, the Mutual Information is defined as:

$$MI(A, B) = H(A) + H(B) - H(A, B) \quad (1)$$

where  $H(A)$  and  $H(B)$  are the entropy of images A and B, and  $H(A, B)$  is the intersection of the entropies, corresponding to a measure of diffusion of joint histogram  $p(a, b)$ . In other words,  $H(A, B)$  is the probability of incidence of the gray value a in image A and the grey value b in image B (in correspondent coordinates), for all a and b in the region of superposition of A and B.

The classic Shannon entropy is given by Equation (2):

$$H = -k \sum_{i=1}^W p_i \log p_i \quad (2)$$

This formalism is restricted to the statistics of the Boltzmann-Gibbs-Shannon (BGS) validity domain, assuming to describe nature for the effect of short ranged interactions and the microscopic memory. Usually, systems that conform to the BGS are referred to as additive systems. Considering that we can decompose a physical system into statistically independent A and B subsystems, the probability of a composite system is:

$$p^{A+B} = p^A * p^B \quad (3)$$

Thus, Shannon entropy demonstrates the additive property:

$$S(A + B) = S(A) + S(B) \quad (4)$$

However, for certain classes of physical systems that possess long range interactions, long time memories, and fractal-type structure it is necessary to extend the Shannon theory. The importance of fractal geometry in medical image processing is explained by the self-similarity observed in biological structures imaged with a finite resolution. These images are spectrally and spatially complex, and also

have similarities at different spatial scales [16]. Constantino Tsallis, influenced by multifractal concept, come up with a generalization of BGS statistics based on the generalized form:

$$Sq = k \frac{1 - \sum_{i=1}^W p_i^q}{q-1} \quad (q \in R, S_1 \equiv S_{BG}) \quad (5)$$

where  $k$  is a positive constant,  $W$  is the number of possibilities and the real number  $q$  is the entropic index of non-additivity degree. The Tsallis entropy is identical to BGS entropy in the limit  $q \rightarrow 1$  [18]. Tsallis entropy is non-additive in such a way that for a statistically independent system, the entropy follows the pseudo-additive entropic rule:

$$Sq(A + B) = Sq(A) + Sq(B) + (1 - q) * Sq(A) * Sq(B) \quad (6)$$

Consequently,  $q = 1$  corresponds to additivity,  $q < 1$  corresponds to sub-additivity and  $q > 1$  to super-additivity [19]. So, considering  $Sq \geq 0$  in the pseudo-additive formalism of the previous equation (6), the following entropic classifications are defined:

$$\text{Sub-additivity } (q > 1): Sq(A + B) < Sq(A) + Sq(B)$$

$$\text{Additivity } (q = 1): Sq(A + B) = Sq(A) + Sq(B) \quad (7)$$

$$\text{Super-additivity } (q > 1): Sq(A + B) > Sq(A) + Sq(B)$$

The entropic index  $q$  fluctuates according to the system properties, which includes the long distance correlations and multifractal characteristics, and represents the degree of non-additivity of the system.

Several generalized differential entropies and divergences have been suggested and proven to be efficient for medical image processing applications. Recently, Carvalho [20] studied Hellinger's metric as a nonparametric metric estimator based on the Parzen window in which it was possible to design a new two-stage resampling error bound estimator. Its asymptotic behavior allows use this metric in three or more densities, just like clustering and image processing and analysis. Additionally, previous studies showed satisfactory results using Tsallis Entropy for segmentation [21] and registration [22] in general image databases and in medical images [23–25]. More principles and concepts about registration methods and similarity metrics can be found in Goshtasby [26].

We used the non-additive Tsallis formula to calculate the entropy in the determination of Mutual Information, which was used as a cost function for the registration. This technical note aims to evaluate the Mutual Information using the Tsallis Entropy (MIT) as a new cost function for MRI and SPECT neuroimage registration, in comparison to the set of cost functions traditionally available on SPM8.

## 2. Material and Methods

### 2.1. Computational Resources and Software

The algorithms and the methods were developed in the Center of Imaging Sciences and Medical Physics of the Ribeirão Preto Medical School. An All-in-one HP Omni Pro110 PC (Intel® Core™2 Duo CPU E7500@2.94 GHz, 4.00 GB memory) running a Microsoft OS (Windows 7 Professional) was used. This supported the following softwares: MRICro version 1.40 build 1 was used to convert the image formats, and MatLab 7.12 (R2011a) to run SPM8, which was used to perform the registrations.

## 2.2. Algorithm

The SPM's registration routines were edited and adapted to incorporate the Tsallis Entropy as a new optional cost function for registration. One important feature of this module is the free selection of values for the non-additive parameter; thereupon, this parameter can be adapted according the registration characteristics.

## 2.3. MRI and SPECT Protocols

All procedures were in compliance with Ethics Committee of the Ribeirão Preto School of Medicine (FMRP-USP) guidelines. The selection of morphologically normal MRI and SPECT images for the present research was provided from three volunteers (two women and one man) who gave written informed consent to participate. These subjects were evaluated by a neurologist from the Medical Center of the Ribeirão Preto Medical School, University of São Paulo, Brazil. The MRI and SPECT images were selected according to the following inclusion criteria: (1) the images should be considered normal, with no previous history of inflammation, infection, surgical intervention or neurological insults; and (2) MRI and SPECT should be acquired and processed in the same machines, of the same facility, as described below. Exclusion criteria included: (1) MRI and SPECT images showing even the slightest evidence of voluntary movement; and (2) SPECT images acquired with low count rate. This research project was approved by our Research Ethics Committee (Protocol Number: 9141/2009). Brain SPECT imaging was carried out using 40 mCi (1480 MBq) of the tracer  $^{99m}\text{Tc}$ —ethyl cysteinate diethylester ( $^{99m}\text{Tc}$ -ECD or  $^{99m}\text{Tc}$ -bicisate). Subjects were injected under strictly controlled conditions, with eyes opened and in a quiet semi-darkened room. The dose was injected by the intravenous route just 30 min after the technician had given verbal instructions and volunteer have recovered from the discomfort caused by the establishment of an intravenous line. SPECT images were acquired 60 min after the tracer injection, using a rotating dual-headed gamma camera (SOPHA, SMV, Twinsburg, OH, USA) equipped with a low-energy, high-resolution parallel-hole collimator with the photopeak energy window centered at 140 keV with a width of 20%. Thirty-two projections (30 s per projection) were acquired per head, in a  $128 \times 128$  matrix with a  $\times 2$  zoom, over a 180 degrees orbit, summing up to 75,000 counts/projection/head, and resulting in 64 views obtained at 31 intervals. Filtered back-projection was performed with a low-resolution Butterworth filter with a cutoff frequency of 0.14 cycles per pixel, of order 9. Images were reconstructed and visually analyzed in the orbitomeatal transverse, coronal and sagittal slices. The uniform attenuation correction was performed taking the size of a pixel at 2.55 mm, using the first-order Chang algorithm, and applying an attenuation coefficient of  $0.12 \text{ cm}^{-1}$ .

MRI images were acquired on a Siemens Magnetom Vision unit of 1.5 Tesla (Erlangen, Germany), according to protocols specifically designed for epilepsy studies: (a) High resolution sagittal T1-weighted spoiled gradient recall (SPGR) sequence; (b) Double echo transverse turbo spin echo (TSE) PD-T2-weighted; (c) A pair of fluid-attenuated inversion recovery (FLAIR) sequences, a transverse sequence with 5-mm thick slices and a coronal sequence with 3-mm thick slices angled perpendicularly to the hippocampus; (d) One turbo short-tau inversion recovery (STIR) coronal

sequence through the temporal lobes with thin continuous sections of 2 mm angle perpendicular to the hippocampus. In this study, only the 3D T1-weighted Gradient-Echo MRI sequence was used [27].

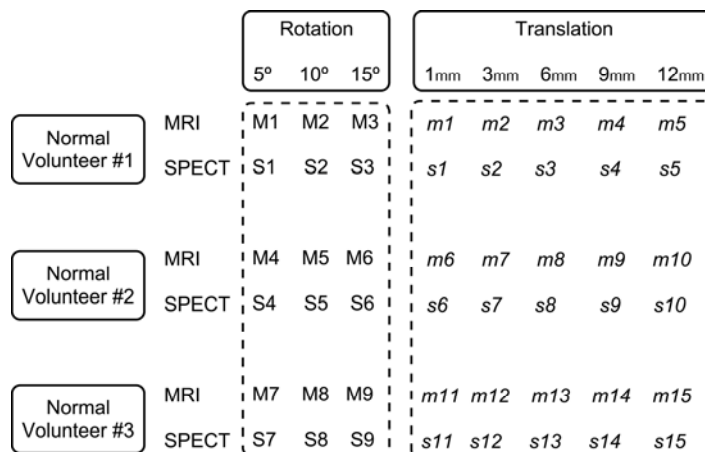
2.4. MRI and SPECT Protocols

The brain SPECT and T1-weighted MRI images were converted from DICOM to NIfIT format using MRicro software (by Chris Rorden, Neuropsychology Lab, Columbia, SC, USA) [28] and then preprocessed using the SPM8 package (Wellcome Trust Centre for Neuroimaging, University College of London, London, UK) [29]. SPM8 was used for the construction of anatomical phantoms containing predetermined geometric variations following the steps: (1) firstly, we verified whether the volumes presented major transformations that could affect the overall performance of the algorithm (for example, 90° rotations). Those that presented these transformations were manually corrected; (2) for each MRI and SPECT volume, the anterior commissure was set as representing the origin volume; (3) the volumes undergone an affine transformation and were co-registered and normalized in the same anatomical space with their respective templates available in the SPM. (SPECT.mnc and T1.mnc); (4) the normalized volumes were binarized using the mask brainmask.mnc, which is also available in the SPM, to remove external signal that could impair the registration process; (5) finally, these normalized volumes were described as MRI\_1, MR\_2 MR\_3 for the respective magnetic resonance volumes of the volunteers #1, #2 and #3, and SPECT\_1, SPECT\_2 SPECT\_3 for the respective SPECT volumes of the volunteers, and usually termed as the base volumes.

2.5. Simulators

Using the baseline volumes, two independent sets of MRI and SPECT simulators were constructed. For the first set (rotational transformation), the baseline MRI and SPECT volumes of each volunteer were used to construct three MRI and three SPECT simulators, which are different among themselves only by the application of 5°, 10° and 15° rotational transformations around the three axes altogether (pitch, roll, and yaw). As a result, we obtained a set of nine rotational MRI (Figure 1, simulators M1 to M9) and 9 rotational SPECT simulators (Figure 1, simulators S1 to S9) for each of the three volunteers.

Figure 1. MRI and SPECT simulators.



For the second set (translational transformation), the MRI and SPECT baseline volumes of each volunteer were used to construct five MRI and five SPECT simulators, which are different among themselves only by the application of 1, 3, 6, 9 and 12 mm of translational transformations around the three axes altogether (pitch, roll, and yaw). As a result, we obtained a set of 15 translational MRI simulators (Figure 1, simulators m1 to m15) and 15 translational SPECT simulators (Figure 1, simulators s1 to s15) for each of the three volunteers. In total, we obtained 48 MRI and SPECT simulators.

Our study was based on rigid transformation because this approach presents wide clinical applicability in neurology and it is effective to describe the spatial relationship between two or more neuroimages since the motion of the brain is largely constrained by the skull. Additionally, similarity metrics measures have proved to perform satisfactory results in linear registration algorithms and several neuroimage softwares, such as SPM, RView and others, use it. Finally, one of the main reasons for the successful impact of rigid registration techniques is the fact that these techniques can be assessed and validate against a gold standard.

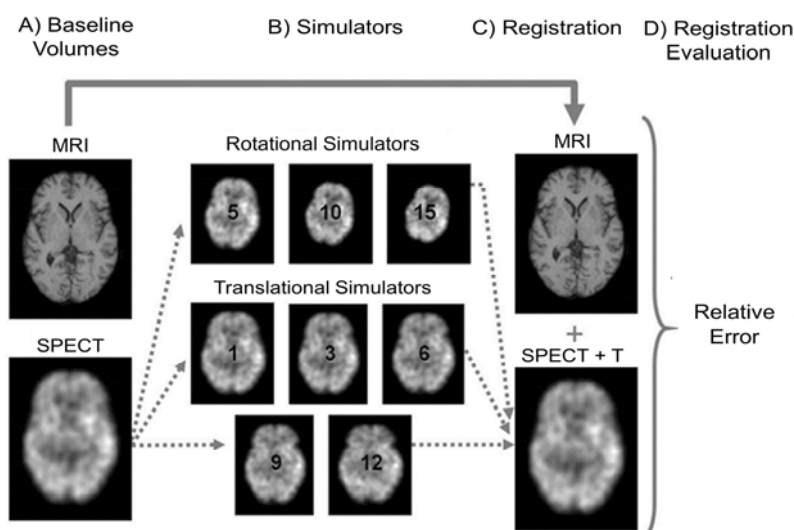
Non-linear registration is also clinically relevant and can use similarity metrics as well. Generally it is useful to relate tissue deformation caused by intervention or relevant changes occurred over time, however it is a more complex approach that has limited validation accuracy and it would not be an appropriate choice to test a new similarity metrics for the first time.

The rotations and translations values for the simulated transformations were defined based on related studies, which generally apply different levels of perturbations in the source image in order to evaluate the registration algorithm under situations that are commonly faced in the clinical scenario. Higher transformations might occur clinically as well, however they can be minimized manually and used as starting point by the algorithm.

## 2.6. Registration

### 2.6.1. Intra-Modality MRI and SPECT Registration

For MRI volumes, the simulators generated from rotational and translational transformations were registered with the respective baseline MRI volumes for each volunteer (see Figure 2). After rigid transformations, the M1, M2 and M3 simulators were registered with the baseline MRI\_1; M4, M5 and M6 simulators with the baseline MRI\_2, and M7, M8 and M9 simulators with the baseline MRI\_3. Also after rigid transformations, the m1 to m5 simulators were registered with the baseline MRI\_1; m6 to m10 simulators with the MRI\_2, and m11 to m15 simulators with the MRI\_3. A total of 336 registrations were performed in this step. For SPECT volumes, the simulators generated from rotational and translational transformations were also registered with their respective baseline SPECT volumes, for each volunteer (See Figure 2). After rigid transformations, the S1, S2 and S3 simulators were registered with the baseline SPECT\_1; S4, S5 and S6 simulators with the SPECT\_2, and S7, S8 and S9 simulators with the SPECT\_3. Also after rigid transformations, the s1 to s5 simulators were registered with the baseline SPECT\_1; s6 to s10 simulators with the SPECT\_2, and s11 to s15 simulators with the SPECT\_3. A total of 336 registrations were performed in this step.

**Figure 2.** Registration pipeline.

### 2.6.2. Inter-Modality Registration

For inter-modality registration, the SPECT simulators generated from rotational and translational transformations were registered with the respective baseline MRI volumes for each volunteer (see Figure 2). After rigid transformations, the S1, S2 and S3 simulators were co-registered with the baseline MRI<sub>1</sub>; S4, S5 and S6 simulators with the MRI<sub>2</sub>, and S7, S8 and S9 simulators with the MRI<sub>3</sub>. Also after rigid transformations, the s1 to s5 simulators were co-registered with the baseline MRI<sub>1</sub>; s6 to s10 simulators with the MRI<sub>2</sub>, and s11 to s15 simulators with the MRI<sub>3</sub>. A total of 336 registrations were performed in this step.

### 2.6.3. Cost Functions for Registrations

In order to perform the intra and inter-modality registrations of the simulators with baseline MRI and SPECT volumes, we used the traditional objective functions (ECC, NCC, NMI and MIS) and random  $q$  values for Tsallis Entropy cost function, using the same computational conditions.

### 2.7. Qualitative and Quantitative Assessments

Upon conclusion of the registrations, we performed a qualitative assessment based on a visual analysis to define which  $q$  values for MIT were able to minimally merge the volumes for intra and inter-modality registrations. For this purpose, we selected only the  $q$  values whose registrations had a visually good alignment. Thus, only those  $q$  values ranging from 0.1 to 3.0 were included as eligible parameters for the following quantitative study. Otherwise, all the traditional objective functions were visually assessed and included in the quantitative study.

For the quantitative assessment, the registration parameters obtained from the rotational and translational transformation matrices were used to calculate the Relative Error (RE) for the respective rotational ( $Sq$ ) and translational ( $t$ -RE) transformations. This RE was obtained for each of the registrations and was calculated as the difference between the ground truth (the expected parameters) and the translational and rotational values returned from the algorithm, divided by the expected parameters.



$$r - RE = \frac{rXexp - rXret}{rXexp} + \frac{rYexp - rYret}{rYexp} + \frac{rZexp - rZret}{rZexp} \tag{8}$$

$$t - RE = \frac{tXexp - tXret}{tXexp} + \frac{tYexp - tYret}{tYexp} + \frac{tZexp - tZret}{tZexp} \tag{9}$$

where the prefixes rX, rY and rZ correspond to the rotations and tX, tY and tZ to the translations performed in the image's axis X, Y and Z, respectively, while suffixes exp means the expected value for the transformation, and ret means the effective returned value by the system.

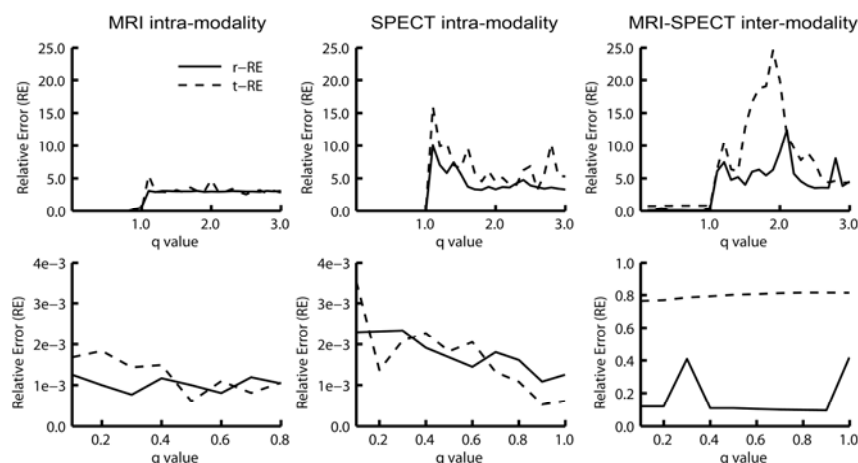
After the individual calculation of r-RE and t-RE for each registration, we calculated an average r-RE and t-RE from simulators registration for each traditional cost function and for each MIT *q* value. Those *q* values that presented the best results (the lowest t-RE and r-RE) were compared against the results of the traditional methods (ECC, NCC, NMI, MIS). This comparison was performed by using the same simulators and computational resources, and by applying the same workflow.

The general overview of the methodology pipeline is showed in Figure 2: (A) Initially, MRI and SPECT volumes were spatially normalized to the same standard space, resulting in two *baseline* MRI and SPECT phantoms; (B) From the *baseline* SPECT volume, eight simulators were built: three produced by applying rotational transformation (with 5, 10 and 15 degrees), and five produced by applying translational transformations (1, 3, 6, 9 and 12 mm); (C) Each simulator was registered to the *baseline* MRI volume and the transformation parameters were recovered; (D) In the final step, transformation parameters were used to estimate the relative error. Intra-modality registrations follow the same pipeline. As it can be noticed, the same procedures were applied to the images of each of the three volunteers, by performing the intra and inter-modality registrations.

### 3. Experimental Section

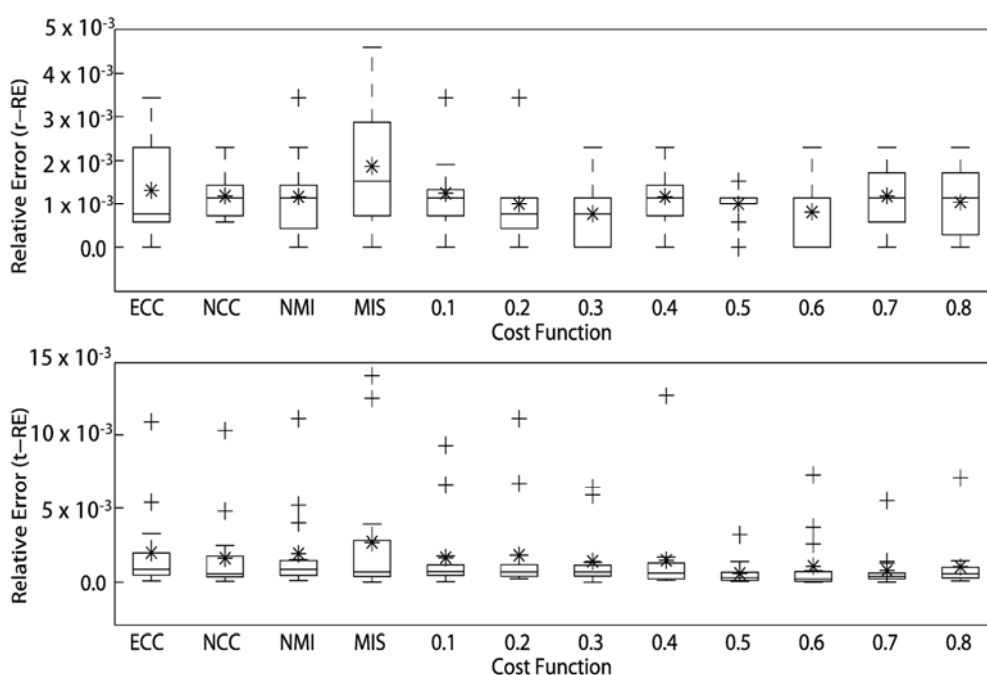
The analysis of the RE of the registrations using Mutual Information based on the Tsallis Entropy revealed that the use of the following *q* values (MIT<sub>*q*</sub>) resulted in the best alignments: 0.1, 0.2, 0.3, 0.4, 0.5, 0.6, 0.7, 0.8, 0.9 and 0.999. For this reason, we selected these *q* values for the comparative analysis between the MIT and the traditional cost functions commonly available in SPM8. Furthermore, we found that *q* values higher than 1.0 resulted in large registration errors (r-RE and t-RE) leading to significant misalignments between simulators, as illustrated in Figure 3.

**Figure 3.** *q* value evaluations based on rotational (r-RE) and translational (t-RE) relative errors.



The RE of the rotational and translational simulations of the cost functions for intra-modality registrations of MRI volumes are presented in Figure 4. The  $MITq = 0.3$  presented the best registration for rotational simulations ( $r\text{-RE} = 7.644290 \times 10^{-4}$ ) and  $MITq = 0.5$  was the best cost function for translational simulations showing  $t\text{-RE} = 6.00741 \times 10^{-4}$ . We also noticed that for rotational simulations, except NCC, all the others cost functions showed at least one registration with  $r\text{-RE} = 0$ . The two best cost functions here ( $MITq = 0.3$  and  $MITq = 0.6$ ) presented three perfect registrations ( $r\text{-RE} = 0$ ). For translational simulations, all cost functions presented at least one registration with  $t\text{-RE}$  very close to 0, however, most part of them presented two or more superior outliers.  $MITq = 0.5$  showed just one superior outlier.

**Figure 4.** Relative Errors for each cost function used for MRI intra-modality registration.



Symbols: + outliers; \* mean, the line inside the boxplot is the median.

Next, we analyzed the rotational and translational simulations of the remaining 13 cost functions, and ranked them in a decreasing order according to the relative errors values (See Table 1). The MIT cost functions presented lower r-RE and t-RE than other cost functions in majority of the intra-modality MRI registrations.

The RE of the rotational and translational simulations of the cost functions for intra-modality registrations of SPECT volumes are presented in Figure 5. The  $MITq = 0.9$  presented the best registration for both rotational and translational transformations of SPECT volumes ( $r\text{-RE} = 1.082823 \times 10^{-3}$  and  $t\text{-RE} = 5.2463 \times 10 \times 10^{-4}$ ); followed by the decreasing performance of the NCC,  $MITq = 0.999$ ,  $MITq = 0.8$ ,  $MITq = 0.5$  and NMI for rotational transformations, and the decreasing performance of the  $MITq = 0.999$ ,  $MITq = 0.8$ ,  $MITq = 0.7$ ,  $MITq = 0.2$  and NCC for translational transformations (see Table 2). We also noticed that for rotational simulations, except ECC,  $MITq = 0.5$ ,  $MITq = 0.7$  and  $MITq = 0.8$ , all the others cost functions showed at least one registration with  $r\text{-RE} = 0$ .  $MITq = 0.9$  presented one perfect registration ( $r\text{-RE} = 0$ ) and also the lowest superior limit. For translational simulations all cost functions presented at least one registration with  $t\text{-RE}$  very close to 0, however,

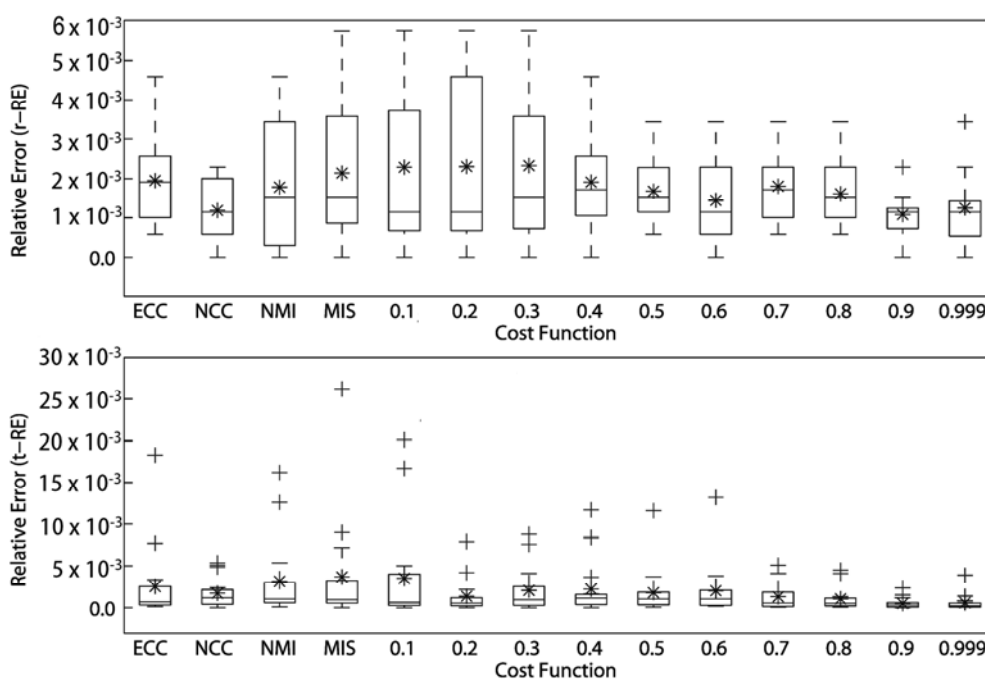
only the MIT<sub>q</sub> = 0.9 exhibited one perfect registration (*t*-RE = 0). MIT<sub>q</sub> = 0.9 showed the lowest superior outliers.

**Table 1.** Ranking of cost functions for intra-modality MRI registration.

Rotation		Translation	
Cost function	<i>r</i> -RE	Cost function	<i>t</i> -RE
MIT <sub>q</sub> = 0.3	$7.6442900 \times 10^{-4}$	MIT <sub>q</sub> = 0.5	$6.00741 \times 10^{-4}$
MIT <sub>q</sub> = 0.6	$8.0681300 \times 10^{-4}$	MIT <sub>q</sub> = 0.7	$8.10741 \times 10^{-4}$
MIT <sub>q</sub> = 0.5	$9.9785900 \times 10^{-4}$	MIT <sub>q</sub> = 0.8	$10.58704 \times 10^{-4}$
MIT <sub>q</sub> = 0.2	$9.9790800 \times 10^{-4}$	MIT <sub>q</sub> = 0.6	$10.95370 \times 10^{-4}$
MIT <sub>q</sub> = 0.8	$10.4043800 \times 10^{-4}$	MIT <sub>q</sub> = 0.3	$14.32407 \times 10^{-4}$
MIT <sub>q</sub> = 0.4	$11.6778600 \times 10^{-4}$	MIT <sub>q</sub> = 0.4	$14.90370 \times 10^{-4}$
NMI	$11.6785900 \times 10^{-4}$	NCC	$16.41481 \times 10^{-4}$
MIT <sub>q</sub> = 0.7	$11.8895400 \times 10^{-4}$	MIT <sub>q</sub> = 0.1	$16.78519 \times 10^{-4}$
NCC	$11.8900300 \times 10^{-4}$	MIT <sub>q</sub> = 0.9	$17.49815 \times 10^{-4}$
MIT <sub>q</sub> = 0.1	$12.5270100 \times 10^{-4}$	MIT <sub>q</sub> = 0.2	$18.33704 \times 10^{-4}$
ECC	$13.1649700 \times 10^{-4}$	NMI	$19.38519 \times 10^{-4}$
MIS	$18.6856500 \times 10^{-4}$	ECC	$20.01852 \times 10^{-4}$
MIT <sub>q</sub> = 0.9	$2486.90042 \times 10^{-4}$	MIS	$26.97407 \times 10^{-4}$
MIT <sub>q</sub> = 0.999	$5621.92037 \times 10^{-4}$	MIT <sub>q</sub> = 0.999	$889.99815 \times 10^{-4}$

Abbreviations: *r*-RE = rotational Relative Error; *t*-RE = translational Relative Error; ECC = Entropy Correlation Coefficient; MIS: Mutual Information using Shannon Entropy; MIT = different *q* values for Mutual Information using Tsallis Entropy; NCC = Normalized Cross Correlation and NMI = Normalized Mutual Information.

**Figure 5.** Relative errors for each cost function used for SPECT intra-modality registration.



Symbols: + outliers; \* mean, the line inside the box plot is the median.

**Table 2.** Ranking of cost functions for intra-modality SPECT registration.

Rotation		Translation	
Cost function	<i>r</i> -RE	Cost function	<i>t</i> -RE
MIT <sub>q</sub> = 0.9	1.082823 × 10 <sup>-3</sup>	MIT <sub>q</sub> = 0.9	5.2463 × 10 <sup>-4</sup>
NCC	1.189027 × 10 <sup>-3</sup>	MIT <sub>q</sub> = 0.999	6.03333 × 10 <sup>-4</sup>
MIT <sub>q</sub> = 0.999	1.25275 × 10 <sup>-3</sup>	MIT <sub>q</sub> = 0.8	10.80741 × 10 <sup>-4</sup>
MIT <sub>q</sub> = 0.8	1.613675 × 10 <sup>-3</sup>	MIT <sub>q</sub> = 0.7	13.16111 × 10 <sup>-4</sup>
MIT <sub>q</sub> = 0.5	1.677276 × 10 <sup>-3</sup>	MIT <sub>q</sub> = 0.2	13.67407 × 10 <sup>-4</sup>
NMI	1.783675 × 10 <sup>-3</sup>	NCC	17.34444 × 10 <sup>-4</sup>
MIT <sub>q</sub> = 0.7	1.804721 × 10 <sup>-3</sup>	MIT <sub>q</sub> = 0.5	18.27593 × 10 <sup>-4</sup>
MIT <sub>q</sub> = 0.4	1.91095 × 10 <sup>-3</sup>	MIT <sub>q</sub> = 0.6	20.49815 × 10 <sup>-4</sup>
ECC	1.953432 × 10 <sup>-3</sup>	MIT <sub>q</sub> = 0.3	20.86111 × 10 <sup>-4</sup>
MIS	2.14404 × 10 <sup>-3</sup>	MIT <sub>q</sub> = 0.4	22.68148 × 10 <sup>-4</sup>
MIT <sub>q</sub> = 0.1	2.292969 × 10 <sup>-3</sup>	ECC	25.63704 × 10 <sup>-4</sup>
MIT <sub>q</sub> = 0.6	2.2935780 × 10 <sup>-3</sup>	NMI	31.63889 × 10 <sup>-4</sup>
MIT <sub>q</sub> = 0.2	2.314478 × 10 <sup>-3</sup>	MIT <sub>q</sub> = 0.1	35.30000 × 10 <sup>-4</sup>
MIT <sub>q</sub> = 0.3	2.33567 × 10 <sup>-3</sup>	MIS	36.73333 × 10 <sup>-4</sup>

Abbreviations: *r*-RE = rotational Relative Error; *t*-RE = translational Relative Error; ECC = Entropy Correlation Coefficient; MIS: Mutual Information using Shannon Entropy; MIT = different *q* values for Mutual Information using Tsallis Entropy; NCC = Normalized Cross Correlation and NMI = Normalized Mutual Information.

All RE of the rotational and translational simulations of the cost functions for inter-modality registrations of MRI and SPECT volumes are presented in Table 3 and Figure 6. The MIT<sub>q</sub> = 0.9 presented the best registration for rotational transformations of the SPECT volumes to MRI (*r*-RE = 9.6244645 × 10<sup>-2</sup>), while the ECC presented the best registration for translational transformations (*t*-RE = 6.94952593 × 10<sup>-1</sup>), followed by MIS (*t*-RE = 7.48891111 × 10<sup>-1</sup>), NMI (*t*-RE = 7.50359259 × 10<sup>-1</sup>) and MIT<sub>q</sub> = 0.1 (*t*-RE = 7.6336963 × 10<sup>-1</sup>). We noticed that for rotational simulations, only MIT<sub>q</sub> = 0.9 and MIT<sub>q</sub> = 0.999 presented *r*-RE = 0 (1 registration), however, MIT<sub>q</sub> = 0.999 had a remarkable superior outlier (*r*-RE = 3) while MIT<sub>q</sub> = 0.9 did not present any outliers. For translational simulations, MIT and traditional cost functions showed similar performance (the lowest mean *t*-RE was 6.94952593 × 10<sup>-1</sup> (ECC) and the highest mean *t*-RE was 8.1523925 × 10<sup>-1</sup> (MIT<sub>q</sub> = 0.9)), however, ECC presented both the lowest superior limit and outliers.

**Table 3.** Ranking of cost functions for inter-modality MRI-SPECT registration.

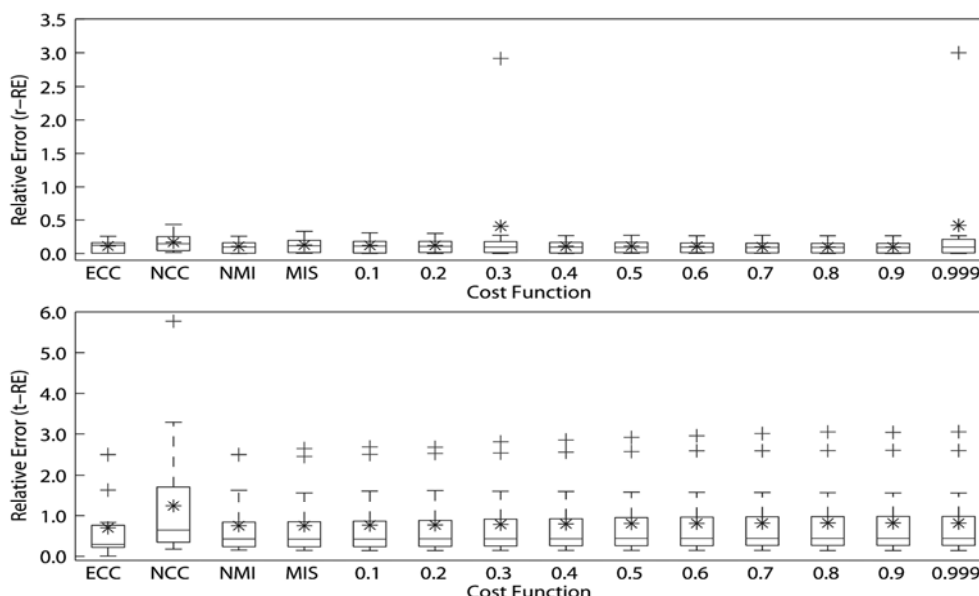
Rotation		Translation	
Cost function	<i>r</i> -RE	Cost function	<i>t</i> -RE
MIT <sub>q</sub> = 0.9	9.6244645 × 10 <sup>-2</sup>	ECC	6.94952593 × 10 <sup>-1</sup>
MIT <sub>q</sub> = 0.8	9.7476227 × 10 <sup>-2</sup>	MIS	7.48891111 × 10 <sup>-1</sup>
MIT <sub>q</sub> = 0.7	10.03424090 × 10 <sup>-2</sup>	NMI	7.50359259 × 10 <sup>-1</sup>
MIT <sub>q</sub> = 0.6	10.3909320 × 10 <sup>-2</sup>	MIT <sub>q</sub> = 0.1	7.6336963 × 10 <sup>-1</sup>
NMI	10.64781780 × 10 <sup>-2</sup>	MIT <sub>q</sub> = 0.2	7.68925556 × 10 <sup>-1</sup>
MIT <sub>q</sub> = 0.4	10.87292010 × 10 <sup>-2</sup>	MIT <sub>q</sub> = 0.3	7.8496963 × 10 <sup>-1</sup>
MIT <sub>q</sub> = 0.5	10.8729323 × 10 <sup>-2</sup>	MIT <sub>q</sub> = 0.4	7.92383889 × 10 <sup>-1</sup>
ECC	11.00871570 × 10 <sup>-2</sup>	MIT <sub>q</sub> = 0.5	8.01386667 × 10 <sup>-1</sup>

Table 3. Cont.

Rotation		Translation	
Cost function	<i>r</i> -RE	Cost function	<i>t</i> -RE
MIT <sub>q</sub> = 0.2	12.01092550 × 10 <sup>-2</sup>	MIT <sub>q</sub> = 0.6	8.06338519 × 10 <sup>-1</sup>
MIT <sub>q</sub> = 0.1	12.04068950 × 10 <sup>-2</sup>	MIT <sub>q</sub> = 0.7	8.12098704 × 10 <sup>-1</sup>
MIS	12.7412762 × 10 <sup>-2</sup>	MIT <sub>q</sub> = 0.999	8.14527963 × 10 <sup>-1</sup>
NCC	16.84977460 × 10 <sup>-2</sup>	MIT <sub>q</sub> = 0.8	8.15023889 × 10 <sup>-1</sup>
MIT <sub>q</sub> = 0.3	40.9058694 × 10 <sup>-2</sup>	MIT <sub>q</sub> = 0.9	8.1523925 × 10 <sup>-1</sup>
MIT <sub>q</sub> = 0.999	41.8411673 × 10 <sup>-2</sup>	NCC	12.44815556 × 10 <sup>-1</sup>

Abbreviations: *r*-RE = rotational Relative Error; *t*-RE = translational Relative Error; ECC = Entropy Correlation Coefficient; MIS: Mutual Information using Shannon Entropy; MIT = different *q* values for Mutual Information using Tsallis Entropy; NCC = Normalized Cross Correlation and NMI = Normalized Mutual Information.

Figure 6. Relative errors for each cost function used for MRI-SPECT inter-modality registration.



### 4. Discussion

The comparative analysis between cost functions assessed in this study evidenced that the Mutual Information method (MIT) using the Tsallis Entropy presented better alignments in five of the six parameters assessed (*i.e.*, MRI and SPECT intra-modality rotational and translational transformations registrations, and the SPECT—MRI inter-modality rotational registration). The MIT did not show the best alignment only for the SPECT—MRI inter-modality translational registration, which was achieved by the ECC.

In the first step, a pilot study was conducted with the objective to identify the range of MIT<sub>q</sub> values that we could use to better investigate the comparison of the MIT with the traditional cost functions. We identified that the best range of *q* values was between 0.1 and 0.999. This finding was of great importance since MIT<sub>q</sub> values higher than 1.0 resulted in significant misalignments. After this preliminary study, we then conducted specific investigations of both rotational and translational transformations applied for each of the intra or inter modality MRI and SPECT registrations.

For intra-modality MRI registration, the MIT using different  $q$  values presented higher performance than the traditional cost functions. These best  $q$  values were 0.3 for rotational and 0.5 for translational MRI registrations. Likewise, Wachowiak *et al.* [30] found that Tsallis Entropy in the Normalized Mutual Information (NMI) presented the best MRI intra-modality alignment, with the difference that the lower errors were obtained with a higher  $q$  value ( $q = 1.1$ ). In their study, the authors used the Euclidean Distance and Root Mean Square (RMS) error to determine the Correctness Ratio (Cr), and results showed that Tsallis Entropy generally had better performance (in terms of producing fewer misregistration) than Shannon NMI for  $q$  value very close to 1 ( $q = 0.9, 1.1$ ) [31]. They argue that the poor performance of low  $q$  values in their study might be due to the use of the Powell optimization method for registration. Nevertheless, we also used Powell's optimization method for 3D-3D MRI registration, and we found that the  $q$  values near 1 has the worst result for both translational and rotational transformations in comparison to the low  $q$  values ranging from 0.3 to 0.5. We believe the difference between these two studies may result from the set of simulators used. Wachowiak *et al.* [32] used 2D-3D registrations while we used 3D-3D ones. Despite this difference, both studies suggest that Tsallis Entropy resulted in best MRI registration performance. This suggests that Tsallis Entropy is a promising method for intra-modality 3D registration, contradicting early studies which indicated the MIS as the best cost function for the intra-modality registrations. Currently, the SPM8 recommends using MIS, NMI and ECC as possible cost functions for inter-modality registrations. For intra-modality registrations, SPM8 allows to use the NCC as an alternative technique, in addition to the aforementioned cost functions [33–36].

Martin *et al.* [24] showed huge improvements using Tsallis entropy in 2D images of MRI T1, MRI T2 and CT. Their algorithm achieved up to seven times faster convergence and four times more precise registration using Tsallis entropy instead of the classic form of entropy using Shannon. The best results were achieved using  $q = 0.7$ , which differs from our results and can be explained by the differences in the image dimensionalities, optimization technique, and registration evaluation method.

Tedeschi *et al.* [25] used Tsallis entropy in fMRI analysis and found that the optimization of  $q$  values restricts the range to  $(-1.0, 0.0)$  and  $(0.5, 1.0)$ , which partially is coincident with our results; their optimum results were found for  $q = 0.7$  and  $-0.5$ .

For intra-modality SPECT registration, the MIT  $q$  values near 1.0 presented higher performance than the traditional cost functions. Interestingly,  $q = 0.9$  resulted in the best performance for both rotational and translational SPECT registrations. As we previously mentioned, SPM8 also recommends MIS, NMI and ECC for both inter and intra-modality registrations. For SPECT and PET images, NMI has been reported to be more stable and robust than MIS for intra-modality SPECT [37] and PET registration [14]. On the other hand, studies have suggested either NCC [22] or other less commonly used algorithms [38] specifically for intra-modality SPECT registrations. Traditionally, correlation coefficients like NCC have shown good performance for intra-modality registrations [39], similar to the findings of our study.

Unfortunately, so far no investigation has evaluated the use of Tsallis Entropy in the SPECT volume registration. We are very interested in finding out what future studies could be carried out using Tsallis Entropy for either SPECT or PET intra-modality registration in order to evaluate its performance in comparison to the traditional cost functions.

For inter-modality MRI and SPECT registrations, both the Tsallis Entropy using  $q = 0.9$  and ECC presented the highest performance for rotational and translational transformations, respectively, when compared to the other traditional cost functions. It was interesting to note that ECC showed better registration performance than MIS, NMI and  $MIT_q$  for the inter-modality registration. In order to verify the accuracy of this result, we repeated our experiment several times and we obtained the same result, *i.e.*, for MRI and SPECT inter-modality registrations, ECC presented smaller translational relative errors than MIS and NMI. In fact, few studies have used ECC for this specific application [40], and the SPM8 also recommends the ECC as a cost function for multi-modality registration. Nonetheless, even though the difference between the relative errors of the translation transformations are small, using ECC and MIS or even  $MIT_q = 0.9$ , for instance, we believe that future studies should be carried out in order to confirm or not if ECC is actually the best cost function for inter-modality translational registrations.

This discussion is important because MIS and NMI have been commonly recommended for inter-modality neuroimaging registrations [41–43]. In comparative studies [44,45], as many as 16 retrospective registration methods from 12 research groups worldwide were evaluated with respect to the MIS and NMI performance in rigid multimodal brain images registration. Ground truth was obtained using bone-implanted skull markers [46]. Their results showed that the two methods that were based on the mutual information outperformed all other methods and reached approximately the same order of accuracy as the gold standard. These comparative studies suggested that the mutual information registration method is suitable for both monomodal and multimodal image registration [14]. It is worth noting that NMI is based on MIS and its performance is similar to MIS to some extent, but with some important differences. NMI is more stable and robust than MIS for both intra- and inter-modality registrations because it is almost an overlap invariant [47]. And this is quite remarkable for PET registrations where MIS often fails. In this setting, and in our study, the Tsallis Entropy presented better alignments than MIS and NMI based on the relative errors. Further studies shall be carried out to evaluate the stability and robustness of the Tsallis Entropy for intra- and inter-modality registrations based on overlapping invariance.

Actually, Tsallis entropy is not a novelty for general medical image registration purposes. Few previous studies had already described the applicability of this non-additive entropy in different image modalities (ultrasound, histological, CT and MRI). However these were quite limited once they were based on single pair of images [25,26]. No extensive analyzes were performed until now.

As strengths of our study, we concentrated the experiments only in MRI and SPECT images, performing 1008 registrations in 48 simulators (336 procedures per registration modality) which provided a considerable number of image processing. Additionally, this is the first study to propose the use of the Tsallis entropy for intra-modality SPECT registration and inter-modality MRI/SPECT registration.

As limitations, our study exhibited a lack of an annotated “ground truth” (landmarks and or labels) on the images, and evaluated a relative small sample of scans, even though we have exhaustively tested the performance of the Tsallis entropy. Considering that fixed landmarks are related to invasive procedures and external landmarks (for example, skin landmarks) are not reliable, here we use well-known geometric transformation as ground truth.

Despite of the limitations described, this study launches a new applicability of the Tsallis Entropy for SPECT registration and its potential contribution for several research and clinical applications. Further studies should be addressed to test this performance of the Tsallis Entropy in real clinical contexts.

Regarding the computation time, all the registrations were done from 100 to 250 s. As expected, intra-modality registrations were faster than the inter-modalities and generally simulators with smaller transformations were more robust as well, however we did not find strong correlations (Pearson Correlation) which could demonstrate relevant improvement in processing time among the cost functions which provided the lowest errors. In the other hand, those cost functions which presented the highest errors generally were slower, since they were not able to converge properly, sometimes they used more iterations looking for the suitable solution, but unsuccessfully.

Since the processing time among the best cost functions were quite similar, it was not considered an important variable in this study, which the main focus was evaluate the registration error.

## 5. Conclusions

We concluded that the Tsallis Entropy showed the highest performance for almost all transformations in the intra and inter-modality MRI and SPECT images registration for the SPM8, except for the translational transformation of the inter-modality MRI and SPECT registration, in which the ECC performed better. If confirmed by further studies, this finding may give rise to many other applications of the Tsallis Entropy for neuroimaging registrations, either for clinical or research purposes. We believe that studies should be addressed to confirm the high performance of the Tsallis Entropy for SPECT and MRI registration or for other neuroimaging modalities like PET and X-Ray Computed Tomography techniques. Additionally, further studies must be carried out to confirm the stability and robustness of the Tsallis Entropy for multi-modality registration, investigating the overlapping invariance.

## Acknowledgments

We gratefully acknowledge the very helpful participation of physicians, colleagues, and technical staff of the Nuclear Medicine Division, Computation and Math Department and the Image Science and Medical Physics Center. The authors also gratefully acknowledge Professor Anthony Finkelstein (Department of Computer Science, University College of London—UCL) for his very helpful comments. *Funding Support:* (a) “São Paulo Research Foundation”—FAPESP, Grants# 2008/03369-7; 2010/10979-6 and 2013/08240-0 (Henrique Tomaz Amaral-Silva); (b) “Foundation of Support to Teaching, Research and Assistance”—(FAEPA) of the Medical Center, Ribeirão Preto Medical School, University of São Paulo—USP, SP, Brazil (Lauro Wichert-Ana and Paulo Mazzoncini de Azevedo-Marques); (c) “The National Council for Scientific and Technological Development” (CNPq), Ministry of Science and Technology, Brazilian Federal Government, Grant# 304255/2010-0 (Paulo Mazzoncini de Azevedo-Marques) and Grant# 305129/2008-2 (Lauro Wichert-Ana); (d) “FINEP/MCT/INFRA—Research and Projects Financing”, Ministry of Science and Technology, Brazilian Federal Government, Grant# 01.09.0117.00, Reference# 0199/08; (e) “Provost’s Office for Research, University of São Paulo—USP”, Núcleo de Apoio à Pesquisa em Neurociência Aplicada—NAPNA—USP, Grant# 2011.1.9333.1.3 (Lauro Wichert-Ana). We confirm that we have read



the Journal's position on issues involved in ethical publication and affirm that this report has the approval of our institutional ethics committee (Process HCRP n° 9241/2009).

### Author Contributions

This research was designed by Lauro Wichert-Ana, Luiz Otávio Murta and Paulo Azevedo-Marques; the research was performed by Henrique Amaral-Silva and Emerson Itikawa; the data analysis was performed by Henrique Amaral-Silva and Emerson Itikawa; and the paper was written by Henrique Amaral-Silva, Lauro Wichert-Ana, Larissa Romualdo-Suzuki and Geraldo Filho Bussato.

### Conflicts of Interest

The authors declare no conflict of interest.

### References

1. Doi, K.; Huang, H.K. Computer-Aided Diagnosis (CAD) and Image-Guide Decision Support. *Comput. Med. Imaging Graph.* **2007**, *31*, 195–197.
2. Azevedo-Marques, P.M.; Oliveira, M.C.; Oliveira, L.F.; Rodrigues, L.C.; Ribeiro, L.T.; Caetano, G.F.; Araújo, D.; Wichert-Ana, L. Free-software in scientific research: NeuroCAD—An open-source neurology computer-aided toolkit. *Braz. J. Biomed. Eng.* **2003**, *19*, 69–75.
3. Hajnal, J.V.; Hill, D.L.G.; Hawkes, D.J. *Medical Image Registration*; the Biomedical Engineering Series; CRC Press: Boca Raton, FL, USA, 2008.
4. Hill, D.L.G.; Batchelor, P.G.; Holden, M.; Hawkes, D.J. Medical Image Registration. *Phys. Med. Biol.* **2001**, *46*, R1–R45.
5. Ashburner, J.; Friston, K.J. Rigid Body Registration. In *Human Brain Function*; Academic Press: Waltham, MA, USA, 2004; pp. 1–18.
6. Gianfranco, L.; Dominietto, M.; Manfreda, I.; Mones, E.; Carriero, A.; Inglese, E.; Krenkli, M.; Brambilla, M. Acceptance Test of a Commercially Available Software for Automatic Image Registration of Computed Tomography (CT), Magnetic Resonance Imaging (MRI) and <sup>99</sup>TmTc-methoxyisobutylisonitrile (MIBI) Single-Photon Emission Computed Tomography (SPECT) Brain Images. *J. Digit. Imaging* **2008**, *21*, 329–337.
7. McNally, K.A.; Paige, A.L.; Varghese, G.; Zhang, H.; Novotny, S.S., Jr.; Spencer, S.S.; Zubal, G.; Blumenfeld, H. Localizing Value of Ictal-Interictal SPECT Analyzed by SPM (ISAS). *Epilepsia* **2005**, *46*, 1450–1464.
8. Maintz, J.B.A.; Viergever, M.A. A Survey of Medical Image Registration. *Med. Image Anal.* **1998**, *2*, 1–37.
9. Oliveira, F.P.M.; Faria, D.B.; Costa, D.C.; Tavares, J.M.R.S. A Robust Computational Solution for Automated Quantification of a Specific Binding Ratio Based on [<sup>123</sup>I]FP-CIT SPECT Images. *Q. J. Nucl. Med. Mol. Imaging* **2014**, *58*, 74–84.
10. Oliveira, F.P.M.; Tavares, J.M.R.S. Medical Image Registration: A Review. *Comput. Methods Biomech. Biomed. Eng.* **2004**, *17*, 73–93.
11. Shannon, C.E. A Mathematical Theory of Communication. *Bell Syst. Tech. J.* **1948**, *27*, 379–423.

12. Collignon, A.; Maes, F.; Delaere, D.; Vandermeulen, D.; Suetens, P.; Marchal, G. Automated Multi-modality Image Registration Based on Information Theory. In Proceedings of the XIVth International Conference on Information Processing in Medical Imaging, Computational Imaging and Vision, Ile de Berder, France, 26–30 June 1995; Springer: New York, NY, USA, 1995; pp. 263–274.
13. Viola, P.; Wells, W.M., III. Alignment by Maximization of Mutual Information. *Int. J. Comput. Vis.* **1997**, *24*, 137–154.
14. Gao, Z.; Gu, B.; Lin, J. Monomodal Image Registration Using Mutual Information Based Methods. *Image Vis. Comput.* **2008**, *26*, 164–173.
15. Pluim, J.P.W.; Maintz, J.B.; Viergever, M.A. Interpolation Artefacts in Mutual Information-Based Image Registration. *Comput. Vis. Image Underst.* **2000**, *77*, 211–232.
16. Lopes, R.; Betrouni, N. Fractal and Multifractal Analysis: A Review. *Med. Image Anal.* **2009**, *13*, 634–649.
17. Tsallis, C. Possible generalization of Boltzmann-Gibbs statistics. *J. Stat. Phys.* **1988**, *52*, 479–487.
18. Dos Santos, R.J.V. Generalization of Shannon's Theorem of Tsallis Entropy. *J. Math. Phys.* **1997**, *38*, doi:10.1063/1.532107.
19. Tsekouras, G.A.; Tsallis, C. Generalized Entropy Arising a Distribution of  $q$  Indices. *Phys. Rev.* **2005**, *71*, 046144.
20. Carvalho, A.R.F.; Tavares, J.M.R.S.; Principe, J.C. A Novel Nonparametric Distance Estimator for Densities with Error Bounds. *Entropy* **2013**, *15*, 1609–1623.
21. Albuquerque, M.P.; Esquef, I.A.; Mello, A.R.G. Image Thresholding Using Tsallis Entropy. *Pattern Recognit. Lett.* **2004**, *25*, 1059–1065.
22. Cvejic, N.; Canagarajah, C.N.; Bull, D.R. Image Fusion Metric Based on Mutual Information and Tsallis Entropy. *Electron. Lett.* **2006**, *42*, 626–627.
23. Diniz, P.R.B.; Murta Junior, L.O.; Brum, D.G.; Araújo, D.B.; Santos, A.C. Brain Tissue Segmentation Using  $q$ -entropy in Multiple Sclerosis Magnetic Resonance Images. *Braz. J. Med. Biol. Res.* **2010**, *43*, 77–84.
24. Martin, S.; Morison, G.; Nailon, W.; Durrani, T. Fast and Accurate Image Registration Using Tsallis Entropy, and Simultaneous Perturbation of Stochastic Approximation. *Electron. Lett.* **2004**, *40*, 595–597.
25. Tedeschi, W.; Muller, H.P.; de Araujo, D.B.; Santos, A.C.; Neves, U.P.C.; Ern e, S.N.; Baffa, O. Generalized Mutual Information fMRI Analysis: A Study of the Tsallis  $q$  Parameter. *Physica A* **2004**, *344*, 705–711.
26. Goshtasby, A.A. *Image Registration: Principles, Tools, and Methods*; Springer: New York, NY, USA, 2012.
27. Crippa, J.A.S.; Zuardi, A.W.; Garrido, G.E.; Wichert-Ana, L.; Guarnieri, R.; Ferrari, L.; Azevedo-Marques, P.M.; Hallak, J.E.C.; McGuire, P.K.; Busatto, G.F. Effects of Cannabidiol (CBD) on Regional Cerebral Blood Flow. *Neuropsychopharmacology* **2004**, *29*, 417–426.
28. Rorden, C. MRICro Software. Available online: <http://www.mricro.com> (accessed on 31 January 2014).
29. SPM8 Package. Available online: <http://www.fil.ion.ucl.ac.uk/spm/> (accessed on 31 January 2014).

30. Wachowiak, M.P.; Smolíková, R.; Peters, T.M. Multiresolution Biomedical Image Registration Using Generalized Information Measures. In Proceedings of the Medical Image Computing and Computer-Assisted Intervention (MICCAI), Montreal, QC, Canada, 15–18 November 2003; pp. 846–853.
31. Wachowiak, M.P.; Smolíková, R.; Tourassi, G.D.; Elmaghraby, A.S. Similarity Metrics Based on Nonadditive Entropies for 2D-3D Multimodal Biomedical Image Registration. In Proceedings of the SPIE of Medical Imaging, San Diego, CA, USA, 16 May 2003; SPIE: Bellingham, WA, USA, 2003; pp. 1090–1100.
32. Wachowiak, M.P.; Smolíková, R.; Zurada, J.M.; Elmaghraby, A.S. An Approach to Multimodal Biomedical Image Registration Utilizing Particle Swarm Optimization. *IEEE Trans. Evol. Comput.* **2004**, *8*, 289–301.
33. Maintz, J.B.A.; Beekman, F.J.; de Bruin, W.; van del Elsen, P.A.; van Rijk, P.P.; Viergever, M.A. Automatic Registration and Intensity Scaling of SPECT brain images. *J. Nucl. Med.* **1996**, *37* (Suppl. 5), 213.
34. Maes, F.; Collignon, A.; Vandermeulen, D.; Marchal, G.; Suetens, P. Multimodality Image Registration by Maximization of Mutual Information. *IEEE Trans. Med. Imaging* **1997**, *16*, 187–198.
35. Viola, P.A. Alignment by Maximization of Mutual Information. Ph.D. Thesis, Massachusetts Institute of Technology, Cambridge, MA, USA, 1995.
36. Wells, W.M., III; Viola, P.; Atsumi, H.; Nakajima, S.; Kikinis, R. Multi-Modal Volume Registration by Maximization of Mutual Information. *Med. Image Anal.* **1996**, *1*, 35–51.
37. Radau, E.P.; Slomka, P.J.; Julin, P.; Svensson, L.; Wahlund, L.O. Evaluation of Linear Registration Algorithms for Brain SPECT and the Error Due to Hypoperfusion lesions. *Med. Phys.* **2001**, *28*, 1660–1668.
38. Pavia, J.; Ros, D.; Catafau, A.M.; Lomeña, F.J.; Huguet, M.; Setoain, J. Three-dimensional Realignment of Activation Brain Single-photon Emission Tomographic Studies. *Eur. J. Nucl. Med.* **1994**, *21*, 1298–1302.
39. Lemieux, L.; Jagoe, R. Effect of Fiducial Marker Localization on Stereotactic Target Coordinate Calculation in CT Slices and Radiographs. *Phys. Med. Biol.* **1994**, *39*, 1915–1928.
40. Itou, T.; Shinohara, H.; Sakaguchi, K.; Hashimoto, T.; Yokoi, T.; Souma, T. Multimodal Image Registration Using IECC as the Similarity Measure. *Med. Phys.* **2011**, *38*, 1103–1115.
41. Gupta, S.; Ramesh, K.P.; Blash, E.P. Mutual Information Metric Evaluation for PET/MRI Image Fusion. In Proceedings of the IEEE National Aerospace and Electronics Conference (NAECON), Dayton, OH, USA, 16–18 July 2008; pp. 305–311.
42. Cahill, G.C. Normalized Measure of Mutual Information with General Definitions of Entropy for Multimodal Image Registration. In Proceeding of the 4th International Workshop, WBIR, Lübeck, Germany, 11–13 July 2010; LNCS 6204, pp. 258–268.
43. Yokoi, T.; Soma, T.; Shinohara, H.; Matsuda, H. Accuracy and Reproducibility of Co-registration Techniques Based on Mutual Information and Normalized Mutual Information for MRI and SPECT Brain Images. *Ann. Nucl. Med.* **2004**, *18*, 659–667.
44. West, J.W.; Fitzpatrick, J.M.; Wang, M.Y.; Dawant, B.M.; Maurer, C.R.; Kessler, R.M.; Maciunas, R.J. Retrospective Intermodality registration techniques for images of the head: Surfaced-based *versus* volume-based. *IEEE Trans. Med. Imaging* **1999**, *18*, 144–150.

45. West, J.W.; Fitzpatrick, J.M.; Wang, M.Y.; Dawant, B.M.; Maurer, C.R.; Kessler, R.M.; Maciunas, R.J.; Barillot, C.; Lemoine, D.; Collignon, A.; *et al.* Comparison and Evaluation of Retrospective Intermodality Brain Image Registration Techniques. *J. Comput. Assist. Tomogr.* **1997**, *21*, 554–566.
46. Maurer, C.R.; Fitzpatrick, J.M.; Wang, M.Y.; Galloway, R.L.; Maciunas, R.J.; Allen, G.S. Registration of head volume images using implantable fiducial markers. *IEEE Trans. Med. Imaging* **1997**, *16*, 447–462.
47. Studholme, C.; Hill, D.L.G.; Hawkes, D.J. An Overlap Invariant Entropy Measure of 3D Medical Image Alignment. *Pattern Recognit.* **1999**, *32*, 71–86.

© 2014 by the authors; licensee MDPI, Basel, Switzerland. This article is an open access article distributed under the terms and conditions of the Creative Commons Attribution license (<http://creativecommons.org/licenses/by/3.0/>).